HIPPOCAMPUS 24:341–353 (2014)

Recognition Memory and Theta–Gamma Interactions in the Hippocampus

John B. Trimper, Roxana A. Stefanescu, and Joseph R. Manns*

Abstract: Neuronal oscillations and cross-frequency interactions in the rat hippocampus relate in important ways to memory processes and serve as a model for studying oscillatory activity in cognition more broadly. We report here that hippocampal synchrony (CA3–CA1 coherence) increased markedly in the low gamma range as rats were exploring novel objects, particularly those for which the rat subsequently showed good memory. The gamma synchrony varied across phases of the theta rhythm such that coherence was highest at the falling slope and trough of the theta wave. Further, the shape of the theta wave was more asymmetric and elongated at the falling slope during exploration of objects for which the rat subsequently showed good memory as compared with objects for which the rat subsequently showed poor memory. The results showed a strong association between event-related gamma synchrony in rat hippocampus and memory encoding for novel objects. In addition, a novel potential mechanism of cross-frequency interactions was observed whereby dynamic alterations in the shape of theta wave related to memory in correspondence with the strength of gamma synchrony. These findings add to our understanding of how theta and gamma oscillations interact in the hippocampus in the service of memory. © 2013 Wiley Periodicals, Inc.

KEY WORDS: hippocampus; recognition memory; oscillations; theta; gamma; coherence

INTRODUCTION

Neuronal oscillations emerge from synchronous fluctuations in ionic currents and help to coordinate interactions between neural networks by modulating spike timing and synaptic plasticity (Buzsáki and Draguhn, 2004; Buzsáki et al., 2012). Oscillations in the theta (6–12 Hz) and gamma (30–90 Hz) ranges have been extensively studied in the rat hippocampus, and these studies have provided insight about how oscillations can coordinate cellular processes related to memory (Buzsáki, 2002, 2005; Csicsvari et al., 2003; Harris et al., 2003; Colgin and Moser, 2010; Jutras and Buffalo, 2010; Fell and Axmacher, 2011). Indeed, due to its tractability for *in vivo*, *in vitro*, and computational modeling studies, the rat hippocampus has become an important experimental model for studying the role of neuronal oscillations in cognition more broadly (Buzsáki and Draguhn, 2004; Kopell et al., 2010; Lisman and Jensen, 2013). For example, interactions between theta and gamma oscillations in the rat hippocampus have been highlighted as a prime example of cross-frequency coupling in neural networks (Lisman, 2005).

Oscillations across a range of frequencies in the gamma band have been observed in the rat hippocampus, and frequency cut-offs and terminology have varied across reports (Buzsáki and Wang, 2012). Nevertheless, there is good evidence for at least two separable ranges of gamma (Bragin et al., 1995), one centered at ~40 Hz, which will be referred to here as low gamma, and one centered at ~80 Hz, which will be referred to here as high gamma. The amplitude and phase of both ranges of gamma have been shown to vary as a function of theta phase (Bragin et al., 1995; Belluscio et al., 2012). In particular, the low gamma oscillation is largest at the falling slope of the theta wave (as recorded in the CA1 pyramidal layer) and is associated with moments of hippocampal synchrony between CA3 and CA1 (Colgin et al., 2009; Carr et al., 2012). Previous studies in rats have related hippocampal gamma oscillations and theta–gamma interactions to memory performance (Montgomery and Buzsáki, 2007; Tort et al., 2009; Shirvalkar et al., 2010; Carr et al., 2012), but the relationship of these oscillations to memory for individual items is not yet fully understood.

In this study, we sought to determine the extent to which event-related gamma synchrony or theta–gamma interactions in the rat hippocampus would relate specifically to memory performance for trial-unique stimuli. We found that hippocampal synchrony (CA3–CA1 coherence) in the low gamma range increased markedly as rats were exploring novel objects, particularly those objects for which the rat subsequently showed good memory. We also found that CA3–CA1 low gamma coherence varied across phases of the theta rhythm, such that coherence was highest at the falling slope and trough of the theta wave. Finally, we found that the shape of the theta wave was more asymmetric and elongated at the falling slope during exploration of objects for which the rat subsequently showed good memory as compared with objects for which the rat subsequently showed poor memory. The results showed a strong association

Department of Psychology, Emory University, Atlanta, Georgia
Additional Supporting Information may be found in the online version of this article.
Grant sponsor: NIH; Grant number: MH079564 (to J.R.M.).
*Correspondence to: Joseph Manns, Department of Psychology, Emory University, 36 Eagle Row, Atlanta, GA 30322. E-mail: jmanns@emory.edu
Accepted for publication 6 November 2013.
DOI 10.1002/hipo.22228
Published online 14 November 2013 in Wiley Online Library (wileyonlinelibrary.com).

between event-related gamma synchrony in the rat hippocampus and item-specific memory encoding and also suggested a novel mechanism of cross-frequency interactions between theta and gamma oscillations in which the shape of the theta wave related to levels of CA3–CA1 synchrony in the low gamma range.

MATERIALS AND METHODS

Subjects

Six male Long-Evans rats were individually housed (12 h light/dark cycle; testing during light phase) with free access to water and were placed on a restricted diet such that they maintained at least 90% of their free-feeding weight (which was ~400 g). All procedures involving rats were approved by the Institutional Animal Care and Use Committee at Emory University.

Novel Object Recognition Memory Task

Rats performed a recognition memory task (Manns and Eichenbaum, 2009) that was based on rats' spontaneous preference for exploring novel objects more so than repeated objects (Ennaceur and Delacour, 1988). Figure 1A shows a schematic illustration of the task. In general, rats encountered new and repeated objects as they completed clockwise laps on a circular track (diameter = 91.5 cm; track width = 7 cm) to obtain a small piece of chocolate on a central runway, irrespective of object exploration. Objects were placed on small retractable platforms on the outside edge of the track in 9 of 12 possible locations (the location at the end of the central runway and the immediately adjacent locations never contained objects). The objects were typically larger than $5 \times 5 \times 5$ cm^3 but smaller than $15 \times 15 \times 15$ cm^3. Rats were exposed to objects during training, but new objects were used during testing.

Data were taken from two test sessions for each rat in which the rat completed up to 24 trials of an object recognition memory test. New objects were used for each trial. Each trial consisted of one lap in which the rat encountered three novel objects at three different locations and a second lap in which one object was replaced by an identical copy in the same location. The analyses reported here focus on objects that were replaced by duplicates in the same location because exploration times of these objects offered a straightforward interpretation of item-specific object recognition memory performance (Ennaceur and Delacour, 1988; Clark and Squire, 2010). The test sessions additionally involved objects that were replaced on the second lap by duplicates in different locations and objects that were replaced by novel objects in the same location. As the task was self-paced, the elapsed time between first and second encounters ranged between ~30 s to 2 min. Rats completed a lap on an empty track in between each trial. Objects were randomly assigned to object conditions and to locations. Performance was recorded and scored using digital video (30 frames/s). The time was recorded when a rat's nose first came within 1 cm of an object, and if the rat explored the object, the time at which exploration ended. A rat was considered to be exploring an object only if the rat was in close proximity and showing evidence of active investigation (i.e., sniffing and directed attention).

Surgery and Positioning of Recording Electrodes

Stereotaxic surgery was performed after rats were deeply anesthetized with isoflurane (1–3% in oxygen) and given buprenorphine (0.05 mg/kg) as an analgesic. Rats were implanted with a chronic recording assembly that contained independently movable tetrodes. Each tetrode consisted of four 12.5-μm nichrome wires whose tips were plated with gold to reduce the impedance to 200 kΩ at 1 kHz. A stainless steel screw implanted in the skull above the cerebellum served as the reference for local field potentials during recording. Following a 1-week recovery period, tetrode positioning in CA1 and CA3 pyramidal layers occurred over several months and was assisted by several electrophysiological hallmarks of CA1 and CA3. A 20–40 μA current was passed through each recording tetrode for 20 s immediately prior to euthanizing the rat, and the resulting brain lesions served as confirmation of tetrode position. Tetrodes were never turned on the day of the recording or between two test sessions. For recordings of local field potentials in both CA1 and CA3, one tetrode in the middle third of each region's transverse axis (from proximal to distal relative to dentate gyrus) of the pyramidal layer was selected to maintain consistency across rats as oscillations in local field potentials may differ by layer and location (Montgomery et al., 2008; Belluscio et al., 2012; Penley et al., 2012). This mid-proximal/distal region in particular was selected because this portion of CA3 projects directly to the same portion in CA1 and because this portion of both regions receives input from both lateral and medial entorhinal cortex (Witter and Amaral, 2004).

Data Acquisition

Local field potentials (sampling rate = 1,500 Hz; bandpass filter = 1–400 Hz) were acquired using the NSpike data acquisition system (nspike.sourceforge.net). For two rats whose recordings included visible 60 Hz electromagnetic noise, a 60 Hz sine wave was fit to each 10 s of local field potential data and then subtracted, impacting a narrow frequency range from ~59.9 to 60.1 Hz.

Data Analyses

Analysis of local field potentials in relation to behavior

Most of the analyses related oscillatory activity to behavior during the object recognition memory task. These analyses focused on local field potentials recorded during novel object

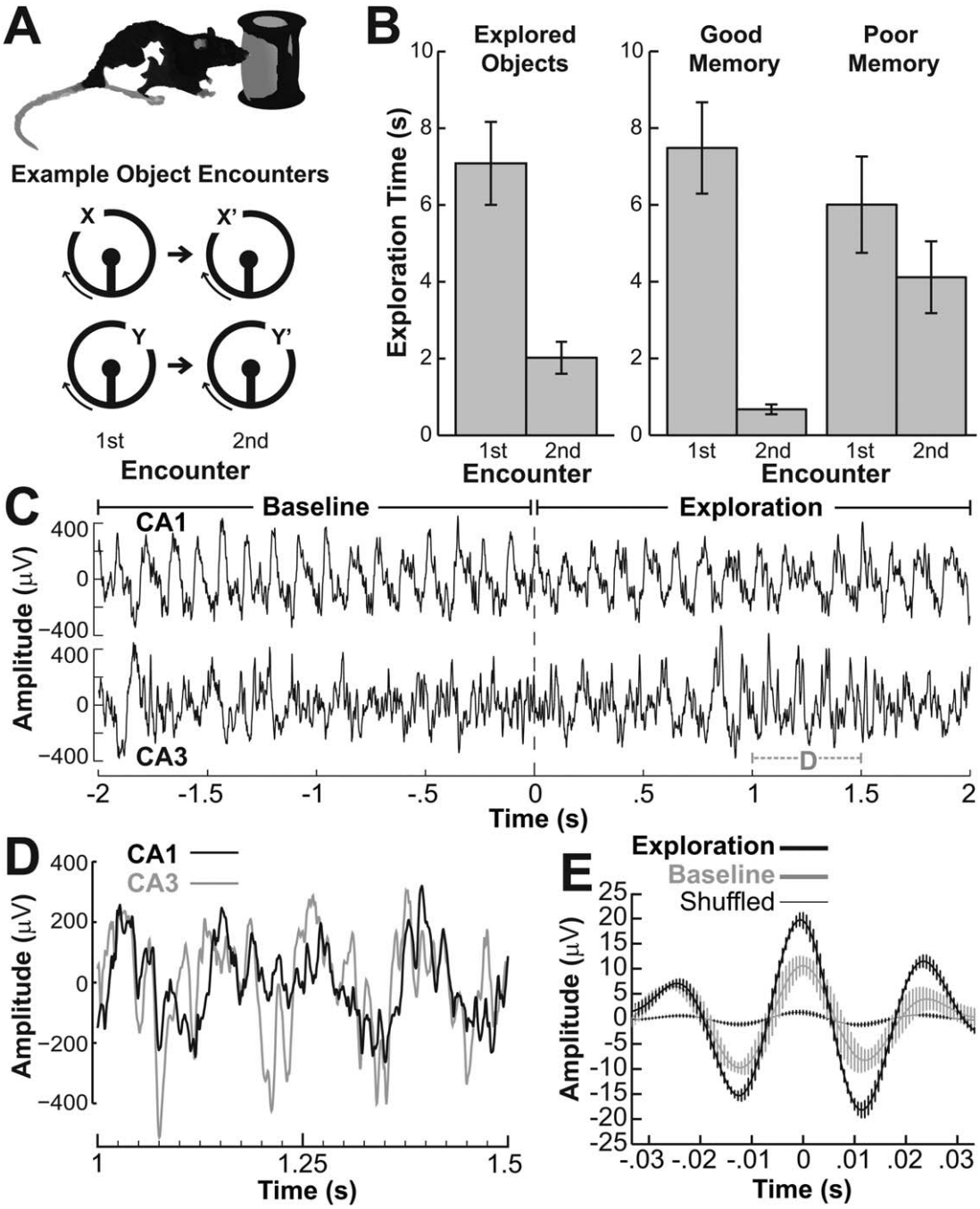

FIGURE 1. Object recognition memory task and example local field potentials from hippocampal regions CA1 and CA3 during object exploration. A: The top illustration depicts a rat exploring an object of a typical size. The bottom schematic shows two examples of first and second encounters with objects on consecutive clockwise laps on the circle track. X′ and Y′ indicate that duplicates of objects X and Y were used for the second encounters. B: The left panel shows mean exploration times for novel objects that were explored for at least 2 s during the first encounter. The reduction in exploration time during the second encounter was taken as evidence for memory of the objects. The right panel shows the same data split by memory performance and shows mean exploration times for object encounters for which the rats showed good performance (defined here as a reduction in exploration time of at least 75% during the second encounter) and poor performance (defined as a reduction that was <75%). Error bars show SEM. C: Example local field potentials recorded simultaneously from CA1 and CA3 during a first encounter with an object (onset at time 0) in which the rat explored the object for >2 s. Theta oscillations are prominent in both regions before and during exploration, and at this scale, gamma oscillations appear as jagged peaks riding on the theta waves. D: An enlarged portion of the local field potentials shown in (C; from time 1 to 1.5 s) more clearly illustrates the presence of gamma oscillations in both CA1 and CA3 as well as the partial alignment between these oscillations. In (D), the field potential from CA3 is plotted with reversed polarity (negative is up) to show better the alignment with the field potential from CA1. E: Local field potentials in CA1 (filtered 30–55 Hz) triggered (time 0) by gamma troughs (local minima < -50 μV in field potentials filtered from 30 to 55 Hz) in CA3 during object exploration and during the 2-s pre-exploration baseline period. The lines and error bars show the mean and SEM across six rats during all exploration events (>2 s). The presence of an ~40 Hz oscillation is especially apparent in the triggered field potential from CA1 during object exploration. The thin line near 0 μV shows similar plots of CA3 gamma-triggered CA1 local field potentials during object exploration, except that CA3 and CA1 field potentials were randomly shuffled between object encounters, indicating that the 40 Hz oscillation did not occur simply as a result of a narrowly filtered signal.

encounters during the first lap of each trial and split the data into good and poor memory conditions based on performance during the second encounters with those objects on the subsequent lap. This subsequent memory approach had the advantage that gross behavior was similar between memory conditions at the time that the neural data was recorded. The definition of good memory performance was based on exploration times of previous experiments using a similar task (Ennaceur and Delacour, 1988; Manns and Eichenbaum, 2009) and on the observation that the criterion permitted inclusion of multiple object encounters in both memory conditions for all rats. All analyses were conducted using MATLAB (MathWorks, Natick, MA).

Analyses of local field potentials were assisted by an open-source library of functions that implemented a multitaper fast Fourier transform method for calculating coherence and other spectral estimates (Bokil et al., 2010). The multitaper approach was used because it has several advantages over a standard (single taper) fast Fourier transform, including reduced variance and bias in the resulting spectral estimates (Bokil et al., 2010). For a sample of local field potentials of duration T seconds, $2TW-1$ orthogonal tapers [discrete prolate spheroidal sequences, also referred to as Slepian sequences; (Slepian, 1978)] were used that were well concentrated in the frequency bandwidth $-W$ to $+W$. Unless noted otherwise, sliding 0.5 s windows with step size of 0.05 s were used to calculate coherence and other spectral estimates during object encounters to reduce the possible complication of nonstationarity in the data (Mitra and Pesaran, 1999). A frequency half bandwidth of 6 Hz (-6 Hz to $+6$ Hz) was used unless noted otherwise, enabling the use of five well-concentrated orthogonal tapers for each 0.5 s section of data at each frequency range. The use of a 0.5 s sliding time window resulted in the first and last 0.25 s being cut off in the moving window coherogram plots since the 0.5 s window would have extended outside the data sample for these periods. Line graphs were plotted by averaging moving windows across either the pre-exploration baseline (-2 to 0 s) or exploration periods (0–2 s).

Measures of hippocampal synchrony

In addition to CA3 power, CA1 power, and CA3–CA1 cross spectrum, two different measures of CA3–CA1 oscillatory synchrony were calculated, coherence (e.g., Mitra and Pesaran, 1999) and phase coherence (Hurtado et al., 2004). Both measures reflected the extent to which the phase relationship between oscillations in CA3 and CA1 were consistent across frequency ranges, and coherence additionally reflected changes in the amplitude of oscillations in one or both regions. Thus, the measures were complementary in that coherence included additional information about the amplitude of the oscillations whereas phase coherence provided a more specific measure of phase locking. Coherence was based on phase consistency within each 0.5 s window as well as across trials of the same experimental condition (i.e., explored vs. baseline and good memory vs. poor memory) for the same time period. To permit valid statistical comparisons between conditions, coherence estimates were Fisher transformed, cross spectrum and power estimates were $\log_{10}$ transformed (and multiplied by 10 to convert from bels to decibels), and, with the exception of phase coherence, all estimates were corrected for bias as described previously (Bokil et al., 2007). The transformed and bias-corrected coherence estimates differed only slightly from the original estimates, and thus we continued to refer to these adjusted values simply as coherence. Phase coherence in comparison reflected the phase consistency of oscillations in CA3 and CA1 within each trial. Specifically, a CA3–CA1 phase offset (Φ) was calculated for each frequency bin across 0.5 s moving windows for each trial using a multitaper fast Fourier transform approach and then represented as a vector ($e^{i\Phi}$). Similar to previous reports (Hurtado et al., 2004), for each 2 s exploration and baseline period, the phase coherence was then calculated as the squared complex magnitude of the mean resultant vector, resulting in a number that ranged from 0 (no phase consistency) to 1 (perfect phase consistency). As this measure used the same amount of data (2 s time windows) for each calculation, and therefore was not differentially impacted by bias between conditions, no bias correction was used for phase coherence.

To assess the statistical significance of differences between conditions for both moving window coherograms and line graphs, a random permutation approach that controlled for the family-wise error rate was used as described previously (Maris and Oostenveld, 2007; Maris et al., 2007). Briefly, for all 2^6 possible ways to partition the six rats' data into two object groups (explored vs. baseline and good memory vs. poor memory), difference plots similar to actual data were created. An initial threshold of 0 ± 2 standard deviations of the original difference plot was used to identify clusters in each permutation. The absolute value of the within-cluster sum was calculated for every cluster, and the maximum cluster value was obtained for every permutation. Only clusters in the original plot whose sum exceeded the 95th percentile value of these maximum cluster values were identified as being statistically significant (i.e., two-tailed $P < 0.05$).

Gamma oscillations in relation to theta phase and shape

Several analyses were conducted to measure the extent to which gamma oscillations showed interactions with theta oscillations. To obtain estimates of theta phase that reflected the non-sinusoidal shape of the theta waveform, theta phase was obtained from the CA1 field potential using a waveform-based method similar to that used previously by others (Belluscio et al., 2012). Briefly, the local field potential from the CA1 tetrode was filtered from 6 to 12 Hz, and timestamps were obtained for all peaks, falling zero crossings, troughs, and rising zero crossings. These timestamps were then revised by filtering anew the CA1 local field potential from 3 to 25 Hz and by finding the nearest matching extrema or zero crossing in this more widely filtered signal. Phase values of 0°, 90°, 180°, and

270° were assigned to these refined peaks, falling zero crossings, troughs, and rising zero crossings, respectively, and quartiles were defined as the range of phases centered on these quarter points and extending halfway to the timestamp of each adjacent quarter point. Thus, although each quartile covered 90°, the actual duration of each quartile could differ.

For the same time period of novel object exploration as used to measure average gamma coherence for each theta quartile (0.5–1.5 s; see below), measurements of the theta wave asymmetry in both memory conditions were obtained by first calculating the mean proportional duration of each theta quartile. Statistical tests could not be performed on these proportional data as proportions across quartiles were interdependent. Thus, the proportions were converted to a distribution of cumulative proportions, and the data were expressed as the difference between the observed cumulative distribution and the cumulative distribution representing a symmetric sine wave. To quantify the overall asymmetry and to permit statistical evaluation of group differences, the area between the observed line for each memory group and the symmetric line was calculated for each rat. Group differences were then assessed with a paired-sample *t*-test. In a related analysis, to calculate the extent to which the theta phase was related to the amplitude of higher frequencies (see Supporting Information Fig. S6), a phase-amplitude modulation index was calculated as described previously (Tort et al., 2010).

The overall modulation of gamma amplitude by theta phase across the entire recording session was estimated similarly to previous reports (Colgin et al., 2009; Belluscio et al., 2012) and required filtering the local field potentials to specific frequency ranges. We adopted definitions of the low (30–55 Hz) and high (65–90 Hz) ranges of gamma that maximized overlap between previous definitions and avoided possible contamination by 60 Hz electromagnetic noise or by >100 Hz power spectra possibly related to spiking activity. For each range, gamma peaks greater than two standard deviations above the mean in the filtered local field potential were counted and peak counts were binned by waveform-based theta phase as recorded in CA1. Standardized peak counts (proportion of total peaks) were then averaged across rats for each bin.

To obtain values of low gamma coherence (30–55 Hz) binned by quartiles of the theta phase during object encounters, theta quartile timestamps for the first 16 cycles of theta during novel object exploration were obtained (representing ~2 s). An approach was then used that was similar to the mutitaper fast Fourier transform approach for calculating coherence described above except that a 0.0625 s (1/16 s) window was used and the step size was variable such that each step moved the window to be centered on the next theta quartile timestamp. A fixed duration window was used rather than one with a duration proportional to the actual quartile duration to avoid using different numbers of data tapers (or, alternatively, different frequency bandwidths) for quartiles of different durations. In addition, the duration of the window was chosen to be the shortest window that would still encompass at least two to three cycles of the low gamma oscillation. To compare results between memory conditions, a rat's mean coherence for both conditions during the middle second (0.5–1.5 s) of novel object exploration was obtained for each quartile of the theta phase. A one-way repeated measures ANOVA was conducted for each group separately to ask if each group's coherence values were significantly modulated by theta quartile, and a 2 × 4 repeated measures ANOVA (memory group by theta quartile) was then conducted to ask if a main effect of group or a group by quartile interaction existed.

Identification of sharp wave-associated ripple events

Sharp wave-associated ripple events (Buzsáki et al., 1992) were identified by visual inspection of the wideband (1–400 Hz) local field potentials for each 2 s exploration and baseline period. As the goal of the analysis was to determine if any possible ripple events contributed to the observed gamma coherence, a lenient criterion was used in which any transient (25–100 ms) oscillatory events (120–240 Hz) were labeled as ripple events. To address the possibility of experimenter bias, all of the 226 (113 exploration periods plus 113 baseline periods) 2 s periods of data were randomly shuffled with 226 two-second periods of data taken from rats during periods of sleep or quiet wakefulness and for each of which ripple events were identified by an individual not associated with the study. In comparison with the 5/226 ripple events identified in the baseline and exploration data, 222/226 periods of this comparison data were identified as containing at least one ripple event. The same blind scoring of ripple events was completed independently by a second scorer, and the results were similar (inter-rater reliability = 0.816; 2/226 for exploration and baseline data, 193/226 for control comparison data).

RESULTS

Memory Was Good for Some Novel Objects and Poor for Others

Six rats completed a recognition memory task in which they encountered novel objects as they completed laps on a circular track (see Fig. 1A). Memory for each object was measured by the extent to which voluntary exploration times were reduced when the object was encountered for a second time in the same position on the track. The neural analyses focused on objects that were explored for at least 2 s during the first encounter to ensure that the rats had sufficient opportunity to form a memory for the object. Consistent with many previous reports using a similar task (Ennaceur and Delacour, 1988; Manns and Eichenbaum, 2009; Clark and Squire, 2010; Bass et al., 2012), rats' exploration times were significantly reduced during the second encounter with these objects as compared with the first (see Fig. 1B), evidencing memory for the initial object encounters (mean exploration time ± SEM = 7.09 ± 1.08 s vs. 2.02 ± 0.42 s, for first and second

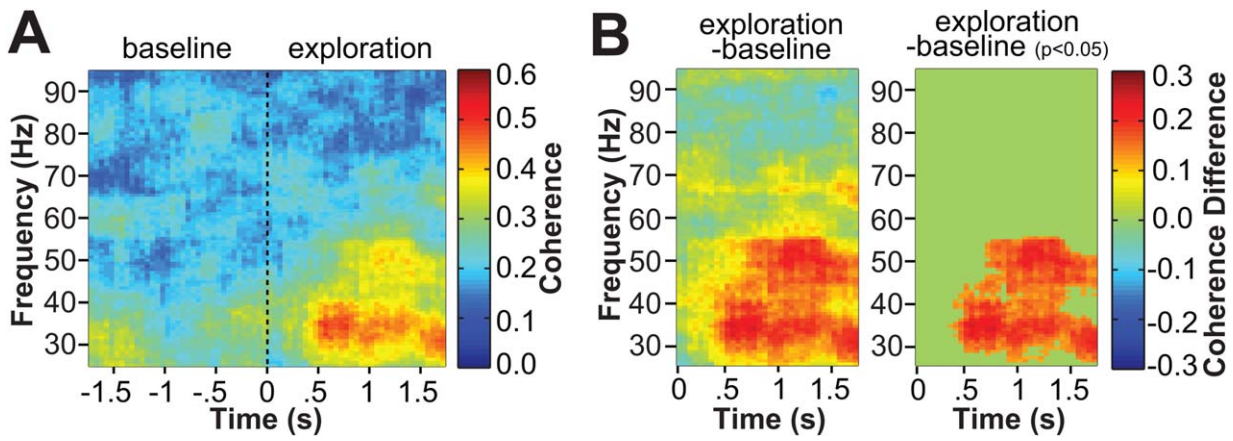

FIGURE 2. Gamma coherence during novel object encounters. A: A sliding window coherogram shows mean CA3–CA1 gamma coherence across rats during encounters with novel objects in which rats explored the objects for at least 2 s. The vertical dashed line at time 0 indicates the time at which the rat first encountered the object. B: The same data are plotted as the difference between gamma coherence during exploration and mean gamma coherence during the pre-exploration baseline period. The right panel shows clusters of data that exceeded statistical significance ($P < 0.05$) when evaluated with a permutation approach that accounted for multiple comparisons (see Materials and Methods section). The results indicate that CA3–CA1 coherence increased in the low gamma range during exploration of novel objects. [Color figure can be viewed in the online issue, which is available at wileyonlinelibrary.com.]

encounters, respectively; paired *t*-test: $t[5] = 6.45$, $P = 0.001$). As a precursor for neural analyses, we additionally sought to separate object encounters into those for which the rats showed good memory performance (defined here as a reduction in exploration time of at least 75% during the second encounter) and poor memory performance (defined as a reduction that was <75%). This partitioning was based in part on previous results from a similar task (Manns and Eichenbaum, 2009) and necessarily led to a larger reduction in exploration times during the second encounter for the objects for which the rats showed good memory (mean exploration time ± SEM = 7.49 ± 1.19 s and 0.67 ± 0.13 s, for first and second encounters respectively—a 91% reduction) as compared with the objects for which the rats showed poor memory (6.01 ± 1.25 s and 4.12 ± 0.94 s, for first and second encounters, respectively—a 31% reduction). Nevertheless, exploration times for first encounters did not differ significantly between objects in the good memory condition and objects in the poor memory condition ($t[5] = 1.90$, $P = 0.117$), suggesting that differences between the groups of objects related more to memory performance during the second encounter rather than rats' general interest in the objects.

Coherence Between CA3 and CA1 Increased in the Low Gamma Range When Rats Explored Novel Objects

Figures 1C,D show examples of theta and gamma oscillations in local field potentials recorded from CA3 and CA1 before and during novel object exploration. Figure 1E suggests that the peaks of CA1 oscillations in the low gamma range tended to align with the troughs of CA3 oscillations in the same range, particularly during exploration of novel objects. To evaluate the extent to which these oscillations were synchronous before and during these object encounters, coherence values were obtained using a method based on multitaper fast Fourier transforms (see Materials and Methods section) and were Fisher-transformed and bias-corrected to permit statistical comparisons between conditions (Bokil et al., 2007). Figure 2 shows CA3–CA1 gamma coherence as a function of time of exploration onset for initial object encounters during which the rat explored the object for at least 2 s (mean number of objects per rat ± SEM = 18.8 ± 4.0). A random permutation approach (Maris and Oostenveld, 2007; Maris et al., 2007) was used to compare exploration (0–2 s) periods to pre-exploration baseline (−2 to 0 s) periods and indicated that a robust and statistically significant increase in CA3–CA1 coherence in the low gamma range occurred shortly after rats initiated exploration of novel objects (Fig. 2B). Figure 3 shows the results for coherence, as well as for phase coherence (a complementary measure of phase consistency; Hurtado et al., 2004), cross spectrum, CA3 power, and CA1 power as a difference between exploration and the pre-exploration baseline across a broad range of frequencies (1–100 Hz). Differences between conditions were again evaluated using a random permutation approach, and the results indicated that the increase in low gamma coherence coincided with a statistically significant increase in CA3 power and CA3–CA1 cross spectrum in the low gamma range in addition to a statistically significant increase in the phase coherence between CA3 and CA1 in the low gamma range. No statistically significant differences were observed in any of the measures outside of the low gamma range.

Several additional analyses were conducted to explore further the increase in CA3–CA1 coherence in the low gamma range observed during object exploration. First, although evidence of

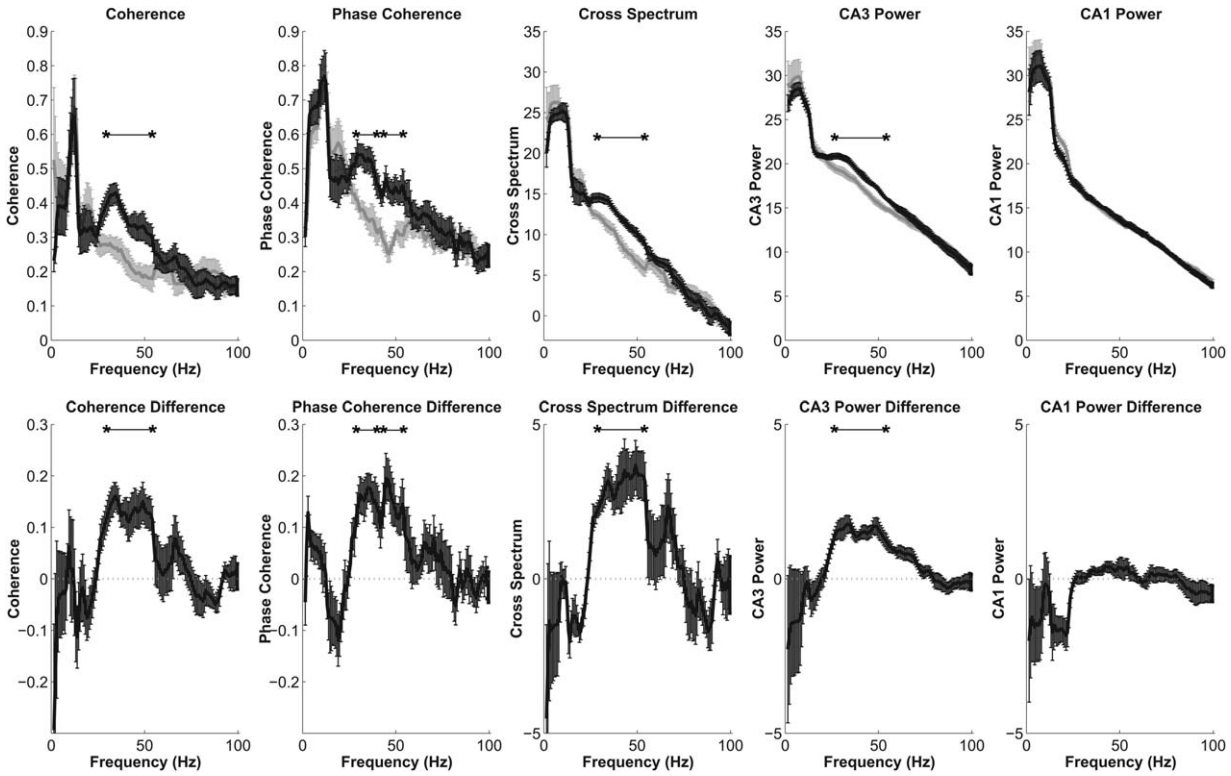

FIGURE 3. Coherence and additional spectral estimates during novel object encounters. The top row of panels shows mean coherence, phase coherence, cross spectrum, CA3 power, and CA1 power for exploration (black lines) and pre-exploration baseline (gray lines) periods for a wide range of frequencies (1–100 Hz). The bottom row shows the mean difference for the same estimates between exploration and baseline periods. Asterisks repeated in both rows denote frequency ranges that differed significantly between exploration and baseline conditions when evaluated with a permutation approach that accounted for multiple comparisons (see Materials and Methods section). Error bars show SEM.

oscillations in CA1 in the low gamma range was apparent during object exploration as transient and intermittent events in individual local field potentials (see Figs. 1C–E), no obvious peak in the CA1 power spectrum in the low gamma range was clearly visible (Fig. 3). Therefore, to ask if the increase in low gamma coherence and phase coherence during object exploration could have resulted from only an increase in CA3 power in the low gamma range, we conducted an additional analysis in which the CA1 local field potential data for each trial was randomly reassigned to a different trial within the same rat, thereby preserving the same overall data set for both CA3 and CA1 (and thus leaving unaffected the respective power spectra) but shuffling the pairings of local field potential data between regions. The coherence and phase coherence estimates for the shuffled data were low across all frequencies, and no differences existed between the exploration and baseline conditions (Supporting Information Fig. S1). Thus, combined with previous evidence that CA3 and CA1 tend to synchronize in the low gamma range (e.g., Colgin et al., 2009), the increases in CA3–CA1 coherence and phase coherence during object exploration appeared to reflect genuine synchrony in the low gamma range between these regions. Second, to ask whether the increase in CA3–CA1 coherence during object exploration could be attributable to cessation of locomotion, the results from object encounters were compared with the instances at the completion of each lap in which the rats stopped to collect a small piece of chocolate reward. A small increase in CA3–CA1 coherence in the low gamma range was observed during these reward collection events, but the level of low gamma coherence was substantially and statistically significantly higher during actual object exploration as determined by comparing the object and reward conditions with a random permutation approach (Supporting Information Fig. S2). Third, to investigate how levels of gamma coherence might change over more extended periods of object exploration, we plotted results for object encounters in which the rat explored the object for over 7 s (7.09 s represented the mean exploration duration) as well as for all explored (>2 s) objects time locked to the offset of exploration (Supporting Information Fig. S3). The results indicated that, although the levels of low gamma CA3–CA1 coherence might have decreased toward the end of exploration, the levels were maintained above-baseline levels throughout exploration. Fourth, although previous results (Carr et al., 2012) suggested that increased CA3–CA1 gamma coherence might occur during sharp-wave associated "ripple" events, we observed very few such events during object exploration (number of 2 s exploration and baseline periods with ripple events = 4 of 113 and 1 of 113, respectively), suggesting that these events contributed

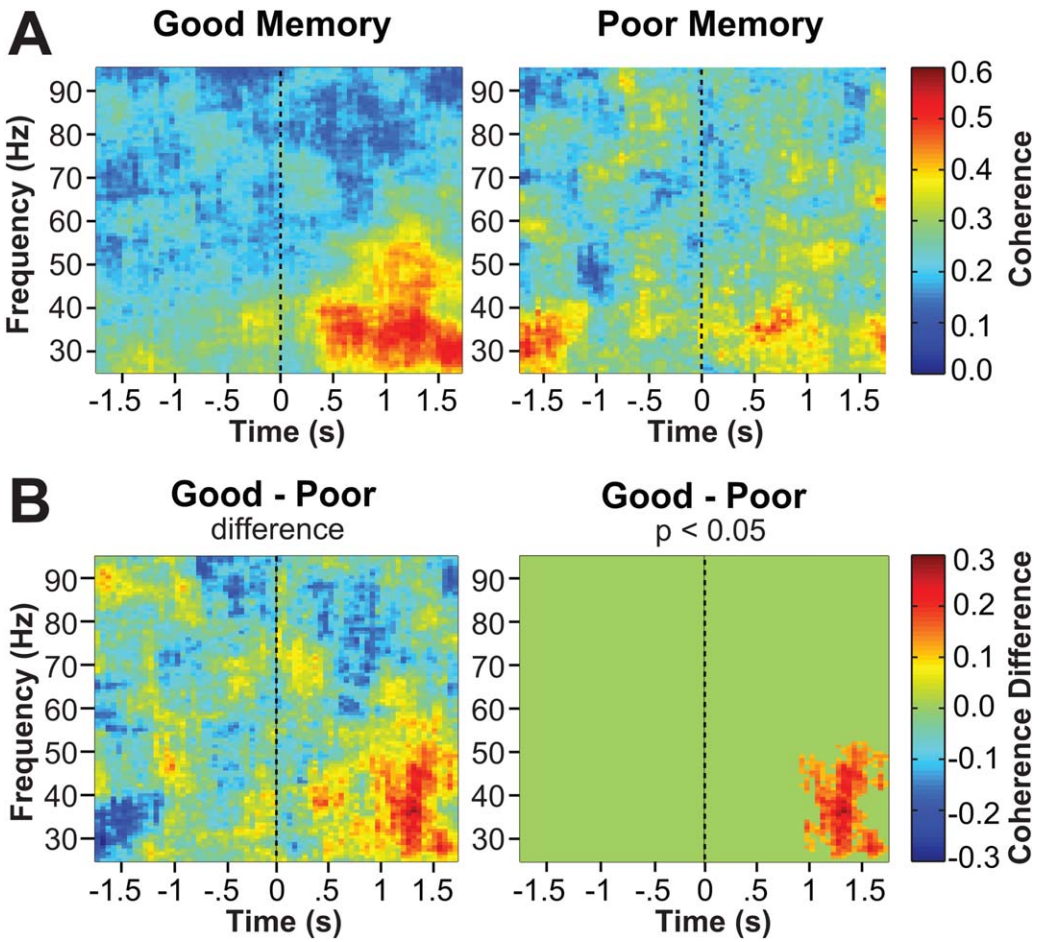

FIGURE 4. Gamma coherence plotted by subsequent memory performance. A: Sliding window coherograms show mean CA3–CA1 coherence across rats in the gamma range for encounters with novel objects explored for at least 2 s split by whether the rats subsequently showed good or poor memory performance. The vertical dashed line in both plots at time 0 indicates the time at which the rat first encountered the object. The increase in CA3–CA1 low gamma coherence during novel object exploration was most pronounced for objects for which the rats subsequently showed good memory. B: The left panel shows the mean difference in CA3–CA1 coherence between encounters with novel objects for which the rats subsequently showed good or poor memory performance. The right panel shows clusters of data that exceeded statistical significance ($P < 0.05$) when evaluated using a permutation-approach that accounted for multiple comparisons (see Materials and Methods section). A cluster in the low gamma range during exploration was the only data to reach statistical significance. Time 0 indicates the time at which the rat first encountered the object. [Color figure can be viewed in the online issue, which is available at wileyonlinelibrary.com.]

little to the present results related to gamma coherence. Although it is unclear exactly what specific aspects of the exploratory behavior related most to the increase in CA3–CA1 gamma coherence (e.g., whisking vs. sniffing), the results indicated that exploration of novel objects was associated with robust increases in hippocampal low gamma synchrony between regions CA3 and CA1.

CA3–CA1 Low Gamma Coherence During Object Exploration Related to Subsequent Memory Performance

Based on previously reported correlations between memory encoding and gamma oscillations in the hippocampus in monkeys and humans (Fell et al., 2001; Sederberg et al., 2007; Jutras et al., 2009), we next asked if the increased coherence in the low gamma range between CA3 and CA1 during novel object exploration corresponded to subsequent memory for the object encounter. Figure 4A shows CA3–CA1 gamma coherence as a function of time of exploration onset for novel object encounters for which the rat explored the object for at least 2 s and subsequently showed good memory performance (mean number of objects per rat $\pm$ SEM $= 11.8 \pm 2.7$) and for which the rat explored the object for at least 2 s yet subsequently showed poor memory performance (mean number of objects $\pm$ SEM $= 7.0 \pm 1.5$). Differences between memory conditions were evaluated using a random permutation approach, and the increase coherence in the low gamma range between CA3 and CA1 was significantly greater for objects for which rats subsequently showed good memory as compared with objects for which the rat

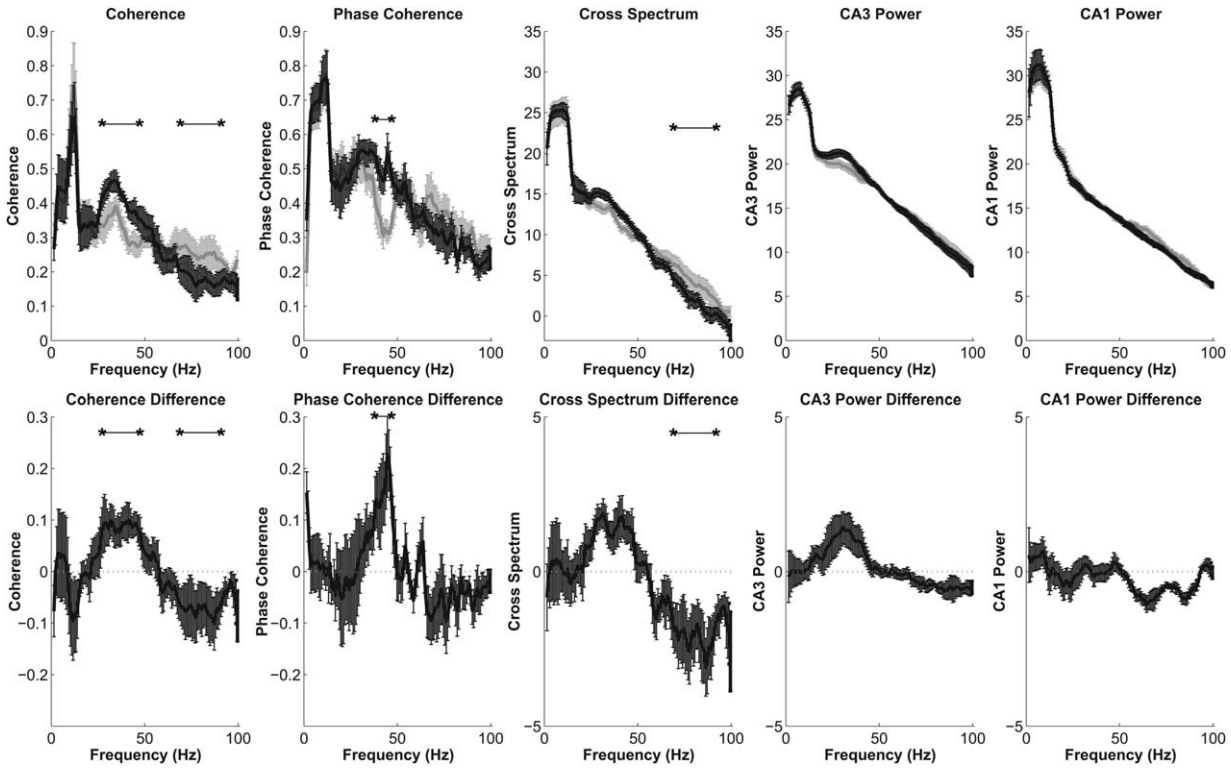

FIGURE 5. Coherence and additional spectral estimates during initial object encounters plotted by subsequent memory performance. The top row of panels shows mean coherence, phase coherence, cross spectrum, CA3 power, and CA1 power for good memory (black lines) and poor memory (gray lines) conditions for a wide range of frequencies (1–100 Hz). The bottom row shows the mean difference for the same estimates between good memory and poor memory conditions. Asterisks repeated in both rows denote frequency ranges that differed significantly between conditions when evaluated with a permutation approach that accounted for multiple comparisons (see Materials and Methods section). Error bars show SEM.

subsequently showed poor memory (Fig. 4B). Figure 5 shows results for coherence, phase coherence, cross spectrum, CA3 power, and CA1 power as a difference between good memory and poor memory conditions across a broad range of frequencies (1–100 Hz). Differences between conditions were again evaluated using a random permutation approach. In addition to a significant increase in coherence and phase coherence in the low gamma range for the good memory versus the poor memory condition, there was also a diffuse yet significant decrease in coherence and CA3–CA1 cross spectrum in the high gamma range. The results are consistent with previous indications that low gamma and high gamma oscillations tend not to occur together in the hippocampus (Colgin et al., 2009) and thus suggest that the increase in low gamma synchrony during the good memory condition might have come at the expense of high gamma synchrony to some extent. The data also indicate that all spectral measures were similar between memory conditions in the frequency range of theta, suggesting via the relationship between theta oscillations and sniffing (Macrides et al., 1982) that differences between memory conditions in the gamma range were not simply due to intensity of exploration. In any case, a key finding was that the extent to which CA3–CA1 synchrony in the low gamma range increased during novel object exploration was associated with good subsequent memory for those objects.

CA3–CA1 Low Gamma Coherence During Object Exploration Differed Across Phases of the Theta Rhythm

Consistent with previous reports (Bragin et al., 1995; Belluscio et al., 2012), we found that the amplitudes of oscillations in the low gamma range (30–55 Hz) in CA1 and CA3 were both modulated by the phase of the theta rhythm in CA1 (see Supporting Information Fig. S4). We therefore asked if CA3–CA1 coherence in the low gamma range also differed by theta phase and whether the profile of gamma coherence across phases of theta might differ by memory performance. Supporting Information Figure S5 shows by quartiles of the theta phase and memory condition CA3–CA1 low gamma coherence during encounters with objects that were explored for at least 2 s. For both groups of objects, CA3–CA1 coherence in the low gamma range was significantly modulated by theta phase (good memory: $F[3,15] = 11.11$, $P = 0.0004$; poor memory: $F[3,15] = 10.83$, $P = 0.0005$) such that coherence was greatest during the falling slope and trough of theta and smallest during the rising slope and peak. In contrast to the overall difference in CA3–CA1 low gamma coherence between good memory and poor memory object conditions, the level of CA3–CA1 coherence in the low gamma range was similar

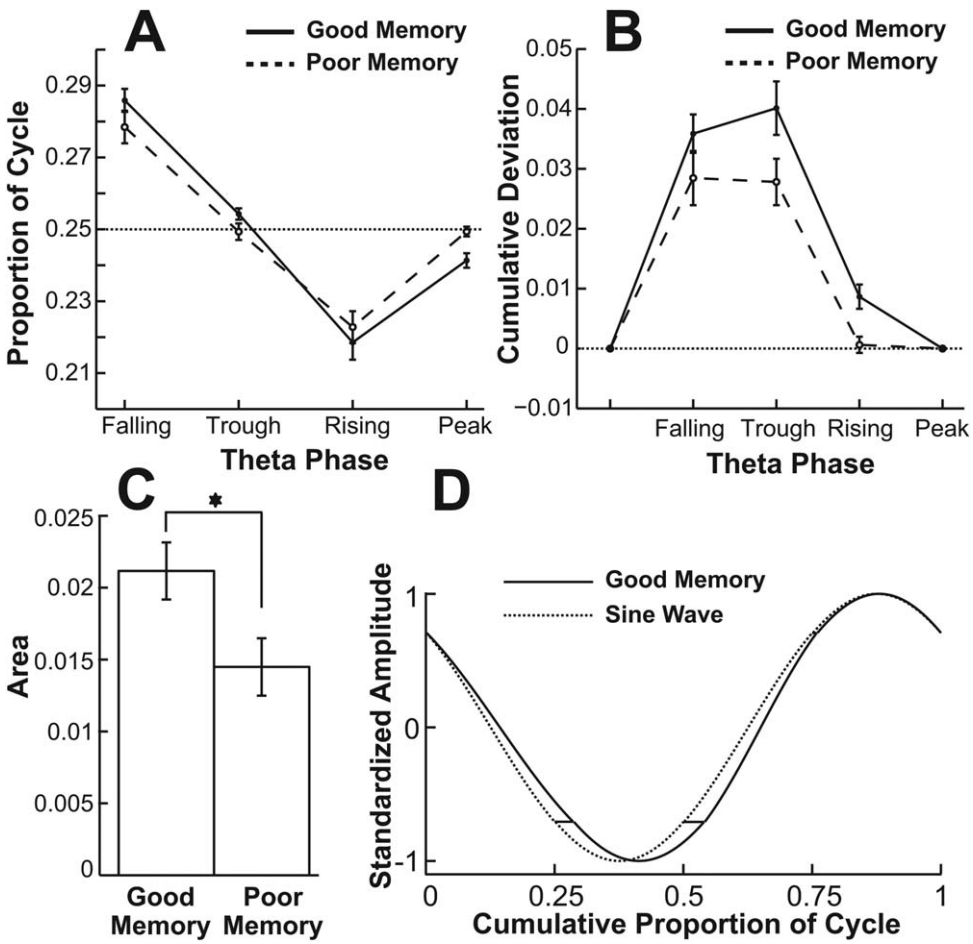

FIGURE 6. Distribution of theta quartile durations during encounters with novel objects split by memory performance. A: Mean duration of each quartile as a proportion of the total cycle. The horizontal dotted line at 0.25 represents the distribution of a symmetric sine wave. For both good memory and poor memory conditions, the observed distribution deviated from symmetry such that the falling slope was disproportionally longer and the rising slope was disproportionately shorter than that of a sine wave. B: Cumulative deviation from symmetry across quartiles of theta cycle. To illustrate the overall asymmetry of the theta wave, the cumulative distribution of theta quartile durations for both memory conditions was plotted as the mean deviation from a symmetric sine wave (indicated by the dotted line at 0). C: Overall asymmetry of theta wave shape during novel object exploration split by subsequent memory performance. The bar graphs show mean area between the cumulative deviation distribution of each memory condition and the distribution of a symmetric sine wave and indicate the overall asymmetry. The theta wave was on average statistically significantly ($P < 0.05$) more asymmetric during exploration of objects for which the rats subsequently showed good memory as compared with objects for which the rats subsequently showed poor memory. Error bars in panels (A–C) show SEM. D: A schematic illustration of the observed mean cumulative asymmetry of the theta wave for the good memory condition (solid line) as compared with a symmetric sine wave (dotted line).

between memory conditions when plotted for each quartile of theta phase (main effect of memory condition: $F[1,5] = 0.35$, $P = 0.578$), and there was no group by quartile interaction ($F[3,15] = 0.35$, $P = 0.791$). We also calculated a modulation index based on previous studies (Tort et al., 2010) that estimated the extent to which the phase of the theta rhythm modulated the amplitude of higher frequency bands (see Supporting Information Fig. S6). Although some differences between good and poor memory conditions were present at high frequencies (~80–180 Hz), a broad range that possibly reflects genuine high frequency oscillations or contributions of spiking to the local field potential (Belluscio et al., 2012; Scheffer-Teixeira et al., 2013), no differences were observed in the low gamma range. Thus, the prominence of low gamma oscillations and coherence differed across the theta cycle but did so similarly for good and poor memory conditions.

The Theta Wave Was More Asymmetric and Elongated at the Falling Slope During Exploration of Objects for Which the Rats Subsequently Showed Good Memory

The shape of the theta wave in the hippocampus has previously been shown to be asymmetric (non-sinusoidal; Buzsáki

et al., 1985) and to differ between behavioral states (awake vs. sleep; Belluscio et al., 2012). Thus, we next asked if the shape of the theta wave might differ between memory conditions. Although peak-to-peak theta frequency did not differ significantly between the memory conditions (mean frequency ± SEM for good memory and poor memory conditions = 7.88 ± 0.10 Hz and 7.95 ± 0.08 Hz, respectively; $t[5] = 0.95$, $P = 0.388$), we nevertheless calculated the duration of each theta quartile as a proportion of the total duration of the theta cycle to ensure that any differences between memory conditions in quartile durations could not be attributed to general frequency differences. Figure 6 shows the duration of each quartile of the theta phase as the mean proportion of the total cycle. Consistent with the previously identified asymmetric shape of the theta wave (Buzsáki et al., 1985; Belluscio et al., 2012), for both memory conditions the distribution of quartile durations differed significantly from that of a symmetric sine wave in which each quartile would account for 25% of the cycle (mean area between observed cumulative distribution and symmetric cumulative distribution ± SEM: good memory condition = 0.021 ± 0.002; $t[5]$ vs. 0 = 10.64, $P = 0.0001$; poor memory condition = 0.014 ± 0.002; $t[5]$ vs. 0 = 7.27, $P = 0.0008$). Statistical tests against symmetry for each quartile were not possible due to the interdependence of proportions across quartiles (i.e., proportions across quartiles necessarily added to 1). However, for both memory conditions, the results suggested that the significantly asymmetric distribution resulted from the falling slope being longer and the rising slope being shorter than one would observe for a symmetric sine wave. In addition, the asymmetry of the theta wave was even greater during exploration of objects for which the rats subsequently showed good memory as compared with objects for which the rats subsequently showed poor memory ($t[5] = 2.57$, $P = 0.0497$). Thus, the greater CA3–CA1 coherence in the low gamma range during exploration of objects for which the rats subsequently showed good memory as compared with poor memory could possibly be understood in part as an elongation of the portion of the theta cycle that contained the greatest amount of gamma synchrony between the two regions.

DISCUSSION

Coherence between CA3 and CA1 increased markedly in the low gamma range when rats initiated exploration of novel objects, and the increase was most pronounced during exploration of objects for which the rat subsequently showed good memory. The increase in coherence was largely sustained throughout the duration of object exploration and appeared to reflect more than simple power increases in CA1 and/or CA3 in the low gamma range, as several analyses indicated that the degree of phase locking between the regions was an important component of the increased CA3–CA1 low gamma coherence. In addition, further analyses suggested that the increased CA3–CA1 coherence in the low gamma range during object exploration was related more to object exploration rather than cessation of locomotion or to sharp-wave associated "ripple" events. Thus, the data indicated that the degree of intrahippocampal gamma synchrony during novel object exploration related most clearly to memory encoding for those objects.

The present results align well with a previous study in monkeys that related successful memory encoding to increased gamma coherence between spikes and local field potentials in the hippocampus (Jutras et al., 2009) and with a previous study in humans that related successful memory encoding to increased gamma coherence between local field potentials in the hippocampus and adjacent entorhinal and perirhinal cortices (Fell et al., 2001). The current findings also build on previous studies in rats that observed coherence between CA3 and CA1 in the gamma range during recurring choice points in spatial memory tasks (Montgomery and Buzsáki, 2007; Carr et al., 2012). Thus, the present results support the view that a transient network state of increased gamma synchrony in the hippocampus correlates with good memory and extend previous work by relating synchrony between CA3 and CA1 specifically in the low gamma range to subsequent memory performance for individual trial-unique stimuli in rats.

Gamma oscillations in many brain regions are important for temporally organizing action potentials and synaptic potentials in local networks (Engel et al., 2001; Fries, 2005; Buzsáki and Wang, 2012). This temporal coordination could benefit CA3–CA1 interactions in the service of memory in at least three ways (Colgin and Moser, 2010): (1) improved fidelity of information coding by organizing patterns of action potentials into "cell assemblies" (Harris et al., 2003), (2) increased efficiency of synaptic transmission by aligning incoming synaptic events with postsynaptic membrane depolarization (Fries, 2005), and (3) enhanced synaptic plasticity by marshalling presynaptic and postsynaptic potentials into the narrow time windows required for spike-timing dependent plasticity (Markram et al., 1997; Bi and Poo, 1998). These mechanisms likely intersect, and all three could support the role of CA3 and CA1 in forming a memory for a specific object encounter.

In addition to suggesting a role for hippocampal oscillations in the low gamma range for trial-unique object memory encoding in rats, the results also provided evidence for a novel type of cross-frequency interaction between gamma and theta oscillations. These results built on several previous studies that observed that the amplitude of gamma oscillations in the hippocampus varied as a function of theta phase (Bragin et al., 1995; Colgin et al., 2009; Belluscio et al., 2012) and two recent studies that noted more specifically that the depth to which theta phase modulated gamma amplitude was related to memory performance in rats (Tort et al., 2009; Shirvalkar et al., 2010). In comparison with those findings, this study found that low gamma oscillations and low gamma coherence varied across theta phases but did so similarly for good memory and poor memory conditions. Instead, the current results suggested that the shape of the theta waveform differed between memory conditions, revealing an elongation of the

portion of the cycle that corresponded to the greatest amount of CA3–CA1 coherence in the low gamma range. Future studies that directly manipulate the theta waveform could help to clarify the manner by and extent to which differences in theta asymmetry could account for the differences in gamma synchrony between memory conditions observed in this study. Nevertheless, taken together with previous results (Buzsáki et al., 1985; Belluscio et al., 2012), the data suggest that future investigations into theta–gamma interactions, and possibly other examples of cross-frequency coupling, should incorporate information about the shape of the oscillations.

Theta oscillations likely benefit temporal coordination in the hippocampus similarly to the three possibilities outlined above for gamma oscillations with the exception that theta oscillations operate at more extended spatial and temporal scales (Buzsáki, 2005). Indeed, there is good evidence that oscillations in these ranges work in concert (Lisman and Jensen, 2013). For example, one view is that interactions between theta and gamma help the hippocampus, particularly region CA1, to separate network states of encoding and retrieval (Colgin and Moser, 2010). By this view, inputs to CA1 from entorhinal cortex represent an influx of information related to external stimuli and inputs to CA1 from CA3 initiate an efflux of information related to retrieved memories (Hasselmo et al., 2002). To reduce interference in CA1, the theta wave partitions these potentially overlapping inputs into different phases of the theta cycle (Hasselmo et al., 2002), each with a different band of preferred gamma synchrony (Colgin et al., 2009). Based on this account, an elongation of the phase of theta at which CA3–CA1 low gamma coherence is maximal would reflect increased time in a network state of memory retrieval. Although this view has been supported by physiological data and models of the hippocampal network (Zilli and Hasselmo, 2006; Manns et al., 2007; Colgin et al., 2009; Carr et al., 2012), it is difficult to reconcile with the results of this study, which suggested a link between CA3 and CA1 low gamma coherence and memory encoding rather than memory retrieval.

One potential reconciliation is that the increased CA3–CA1 low gamma coherence in this study during the initial encounters with novel objects potentially reflected retrieval of relevant contextual information (e.g., previous encounters with similar objects or past moments in the same location) and that this information aided the formation of a new memory for the novel objects. An alternative possibility is that inputs to CA1 from CA3 do not map directly to states of cognition as defined by either encoding or retrieval. Optimal CA3–CA1 LTP induction occurs near the peak of the theta wave (as recorded in the CA1 pyramidal layer), yet maximal CA3–CA1 synaptic input occurs near the trough of the wave (Brankack et al., 1993; Hasselmo et al., 2002; Hyman et al., 2003). Thus, perhaps the falling phase of theta represents a compromise mediated by gamma synchrony between synaptic plasticity and synaptic transmission and that the outcome of this negotiation could benefit either memory encoding or memory retrieval. Further studies will be needed to relate the current results to more mechanistic accounts of synaptic transmission and synaptic plasticity at the CA3–CA1 synapse and to place the synchrony between CA3 and CA1 into a broader framework of network coordination across the extended hippocampal memory system during both memory encoding and retrieval.

Acknowledgments

The authors thank David Bass, Nancy Bliwise, Morgan Brand, Feven Getaneh, Kristin Partain, and Jason Shimiaie for their assistance, Elizabeth Buffalo and Samuel Sober for comments on an earlier version of the manuscript, and Adriano Tort for providing the software for computing phase-amplitude modulation index.

REFERENCES

Bass DI, Partain KN, Manns JR. 2012. Event-specific enhancement of memory via brief electrical stimulation to the basolateral complex of the amygdala in rats. Behav Neuro 126:204–208.

Belluscio MA, Mizuseki K, Schmidt R, Kempter R, Buzsáki G. 2012. Cross-frequency phase-phase coupling between θ and γ oscillations in the hippocampus. J Neurosci 32:423–435.

Bi GQ, Poo MM. 1998. Synaptic modifications in cultured hippocampal neurons: Dependence on spike timing, synaptic strength, and postsynaptic cell type. J Neurosci 18:10464–10472.

Bokil H, Andrews P, Kulkarni JE, Mehta S, Mitra PP. 2010. Chronux: A platform for analyzing neural signals. J Neurosci Methods 192: 146–151.

Bokil H, Purpura K, Schoffelen J-M, Thomson D, Mitra P. 2007. Comparing spectra and coherences for groups of unequal size. J Neurosci Methods 159:337–345.

Bragin A, Jandó G, Nádasdy Z, Hetke J, Wise K, Buzsáki G. 1995. Gamma (40–100 Hz) oscillation in the hippocampus of the behaving rat. J Neurosci 15:47–60.

Brankack J, Stewart M, Fox SE. 1993. Current source density analysis of the hippocampal theta rhythm: Associated sustained potentials and candidate synaptic generators. Brain Res 615:310–327.

Buzsáki G. 2002. Theta Oscillations in the Hippocampus. Neuron 33:325–340.

Buzsáki G. 2005. Theta rhythm of navigation: Link between path integration and landmark navigation, episodic and semantic memory. Hippocampus 15:827–840.

Buzsáki G, Draguhn A. 2004. Neuronal oscillations in cortical networks. Science 304:1926–1929.

Buzsáki G, Wang XJ. 2012. Mechanisms of gamma oscillations. Annu Rev Neurosci 35:203–225.

Buzsáki G, Rappelsberger P, Kellényi L. 1985. Depth profiles of hippocampal rhythmic slow activity ('theta rhythm') depend on behaviour. Electroencephalogr Clin Neurophysiol 61:77–88.

Buzsáki G, Horváth Z, Urioste R, Hetke J, Wise K. 1992. High-frequency network oscillation in the hippocampus. Science (New York, NY) 256:1025–1027.

Buzsáki G, Anastassiou CA, Koch C. 2012. The origin of extracellular fields and currents–EEG, ECoG, LFP and spikes. Nat Rev Neurosci 13:407–420.

Carr MF, Karlsson MP, Frank LM. 2012. Transient slow gamma synchrony underlies hippocampal memory replay. Neuron 75:700–713.

Clark RE, Squire LR. 2010. An animal model of recognition memory and medial temporal lobe amnesia: History and current issues. Neuropsychologia 48:2234–2244.

Colgin LL, Moser EI. 2010. Gamma oscillations in the hippocampus. Physiology 25:319–329.
Colgin LL, Denninger T, Fyhn M, Hafting T, Bonnevie T, Jensen O, Moser M-B, Moser EI. 2009. Frequency of gamma oscillations routes flow of information in the hippocampus. Nature 462:353–357.
Csicsvari J, Jamieson B, Wise KD, Buzsáki G. 2003. Mechanisms of gamma oscillations in the hippocampus of the behaving rat. Neuron 37:311–322.
Engel A, Fries P, Singer W. 2001. Dynamic predictions: Oscillations and synchrony in top-down processing. Nat Rev Neurosci 2:704–716.
Ennaceur A, Delacour J. 1988. A new one-trial test for neurobiological studies of memory in rats. 1: Behavioral data. Behav Brain Res 31:47–59.
Fell J, Axmacher N. 2011. The role of phase synchronization in memory processes. Nat Rev Neurosci 12:105–118.
Fell J, Klaver P, Lehnertz K, Grunwald T, Schaller C, Elger CE, Fernández G. 2001. Human memory formation is accompanied by rhinal-hippocampal coupling and decoupling. Nat Neurosci 4: 1259–1264.
Fries P. 2005. A mechanism for cognitive dynamics: Neuronal communication through neuronal coherence. Trends Cog Sci 9:474–480.
Harris K, Csicsvari J, Hirase H, Dragoi G, Buzsáki G. 2003. Organization of cell assemblies in the hippocampus. Nature 424:552–556.
Hasselmo ME, Bodelón C, Wyble BP. 2002. A proposed function for hippocampal theta rhythm: Separate phases of encoding and retrieval enhance reversal of prior learning. Neural Comput 14: 793–817.
Hurtado JM, Rubchinsky LL, Sigvardt KA. 2004. Statistical method for detection of phase-locking episodes in neural oscillations. J Neurophys 91:1883–1898.
Hyman JM, Wyble BP, Goyal V, Rossi CA, Hasselmo ME. 2003. Stimulation in hippocampal region CA1 in behaving rats yields long-term potentiation when delivered to the peak of theta and long-term depression when delivered to the trough. J Neurosci 23: 11725–11731.
Jutras MJ, Buffalo EA. 2010. Synchronous neural activity and memory formation. Curr Opin Neurobiol 20:150–155.
Jutras MJ, Fries P, Buffalo EA. 2009. Gamma-band synchronization in the macaque hippocampus and memory formation. J Neurosci 29: 12521–12531.
Kopell N, Kramer MA, Malerba P, Whittington MA. 2010. Are different rhythms good for different functions? Frontiers in Human Neuroscience 4:187.
Lisman J. 2005. The theta/gamma discrete phase code occuring during the hippocampal phase precession may be a more general brain coding scheme. Hippocampus 15:913–922.
Lisman JE, Jensen O. 2013. The theta-gamma neural code. Neuron 77:1002–1016.
Macrides F, Eichenbaum H, Forbes W. 1982. Temporal relationship between sniffing and the limbic rhythm during odor discrimination reversal learning. J Neurosci 2:1705–1717.
Manns J, Eichenbaum H. 2009. A cognitive map for object memory in the hippocampus. Learn Mem 16:616–624.
Manns J, Zilli E, Ong K, Hasselmo M, Eichenbaum H. 2007. Hippocampal CA1 spiking during encoding and retrieval: Relation to theta phase. Neurobiol Learn Mem 87:9–20.
Maris E, Oostenveld R. 2007. Nonparametric statistical testing of EEG- and MEG-data. J Neurosci Methods 164:177–190.
Maris E, Schoffelen J-M, Fries P. 2007. Nonparametric statistical testing of coherence differences. J Neurosci Methods 163:161–175.
Markram H, Lübke J, Frotscher M, Sakmann B. 1997. Regulation of synaptic efficacy by coincidence of postsynaptic APs and EPSPs. Science 275:213–215.
Mitra PP, Pesaran B. 1999. Analysis of dynamic brain imaging data. Biophys J 76:691–708.
Montgomery SM, Buzsáki G. 2007. Gamma oscillations dynamically couple hippocampal CA3 and CA1 regions during memory task performance. Proc Natl Acad Sci USA 104:14495–14500.
Montgomery SM, Sirota A, Buzsáki G. 2008. Theta and gamma coordination of hippocampal networks during waking and rapid eye movement sleep. J Neurosci 28:6731–6741.
Penley SC, Hinman JR, Sabolek HR, Escabí M a, Markus EJ, Chrobak JJ. 2012. Theta and gamma coherence across the septotemporal axis during distinct behavioral states. Hippocampus 22: 1164–1175.
Scheffer-Teixeira R, Belchior H, Leão RN, Ribeiro S, Tort ABL. 2013. On high-frequency field oscillations (>100 Hz) and the spectral leakage of spiking activity. J Neurosci 33:1535–1539.
Sederberg PB, Schulze-Bonhage A, Madsen JR, Bromfield EB, McCarthy DC, Brandt A, Tully MS, Kahana MJ. 2007. Hippocampal and neocortical gamma oscillations predict memory formation in humans. Cereb Cortex 17:1190–1196.
Shirvalkar PR, Rapp PR, Shapiro ML. 2010. Bidirectional changes to hippocampal theta-gamma comodulation predict memory for recent spatial episodes. Proc Natl Acad Sci USA 107:7054–7059.
Slepian D. 1978. Prolate spheroidal wave functions, Fourier analysis, and uncertainty—V: The discrete case. Bell Syst Tech J 57:1371–1430.
Tort ABL, Komorowski RW, Manns JR, Kopell NJ, Eichenbaum H. 2009. Theta-gamma coupling increases during the learning of item-context associations. Proc Natl Acad Sci USA 106:20942–20947.
Tort ABL, Komorowski R, Eichenbaum H, Kopell N. 2010. Measuring phase-amplitude coupling between neuronal oscillations of different frequencies. J Neurophys 104:1195–1210.
Witter MP, Amaral DG. 2004. Hippocampal Formation. In: Paxinos G, editor. The Rat Nervous System, 3rd ed. San Diego: Academic Press. pp 635–704.
Zilli EA, Hasselmo ME. 2006. An analysis of the mean theta phase of population activity in a model of hippocampal region CA1. Network 17:277–297.

Figure S1

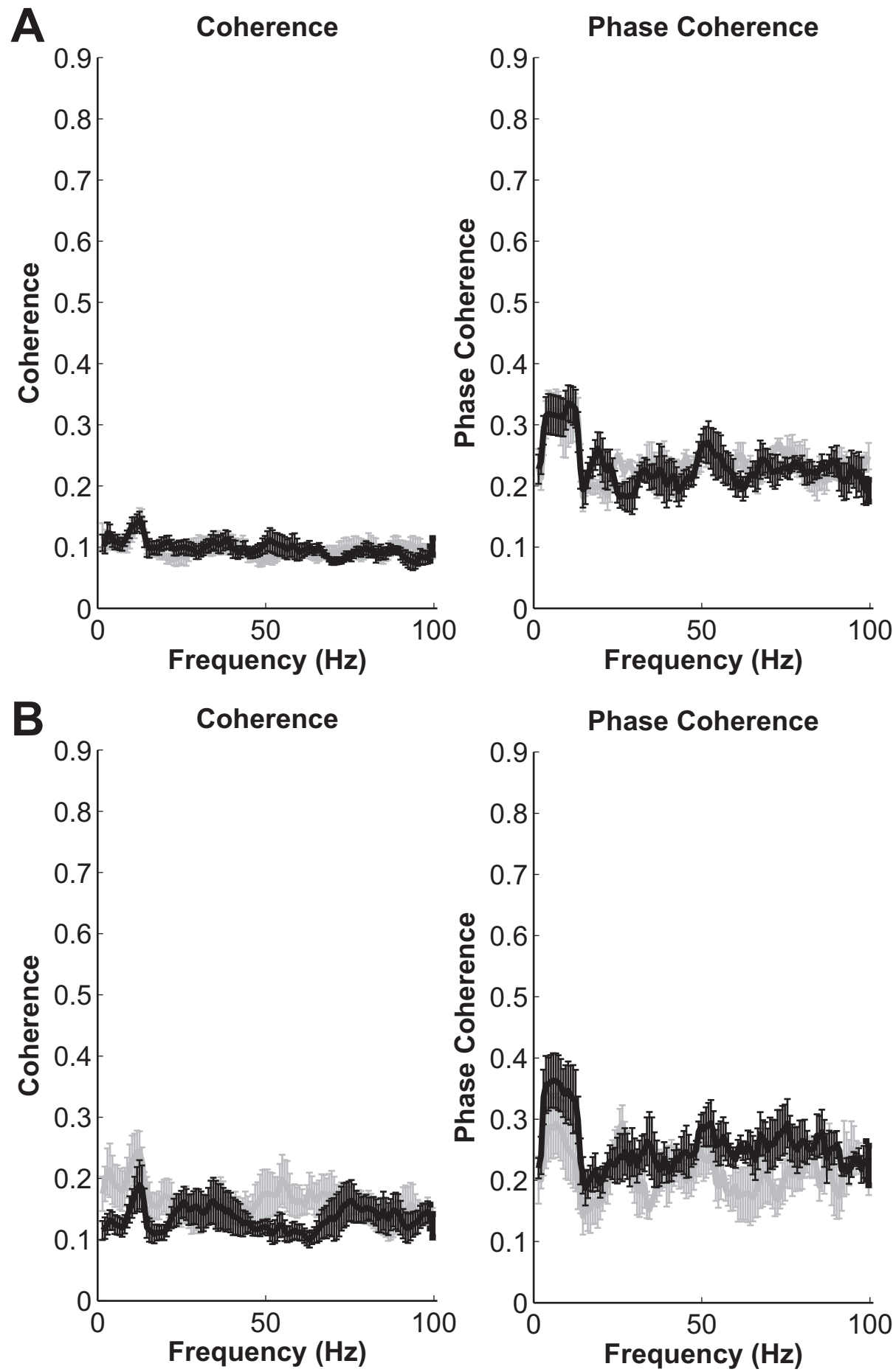
A
Coherence
Phase Coherence
Coherence
Phase Coherence
0.9
0.8
0.7
0.6
0.5
0.4
0.3
0.2
0.1
0
0
50
100
Frequency (Hz)
B
Coherence
Phase Coherence
Coherence
Phase Coherence
Frequency (Hz)

Figure S2

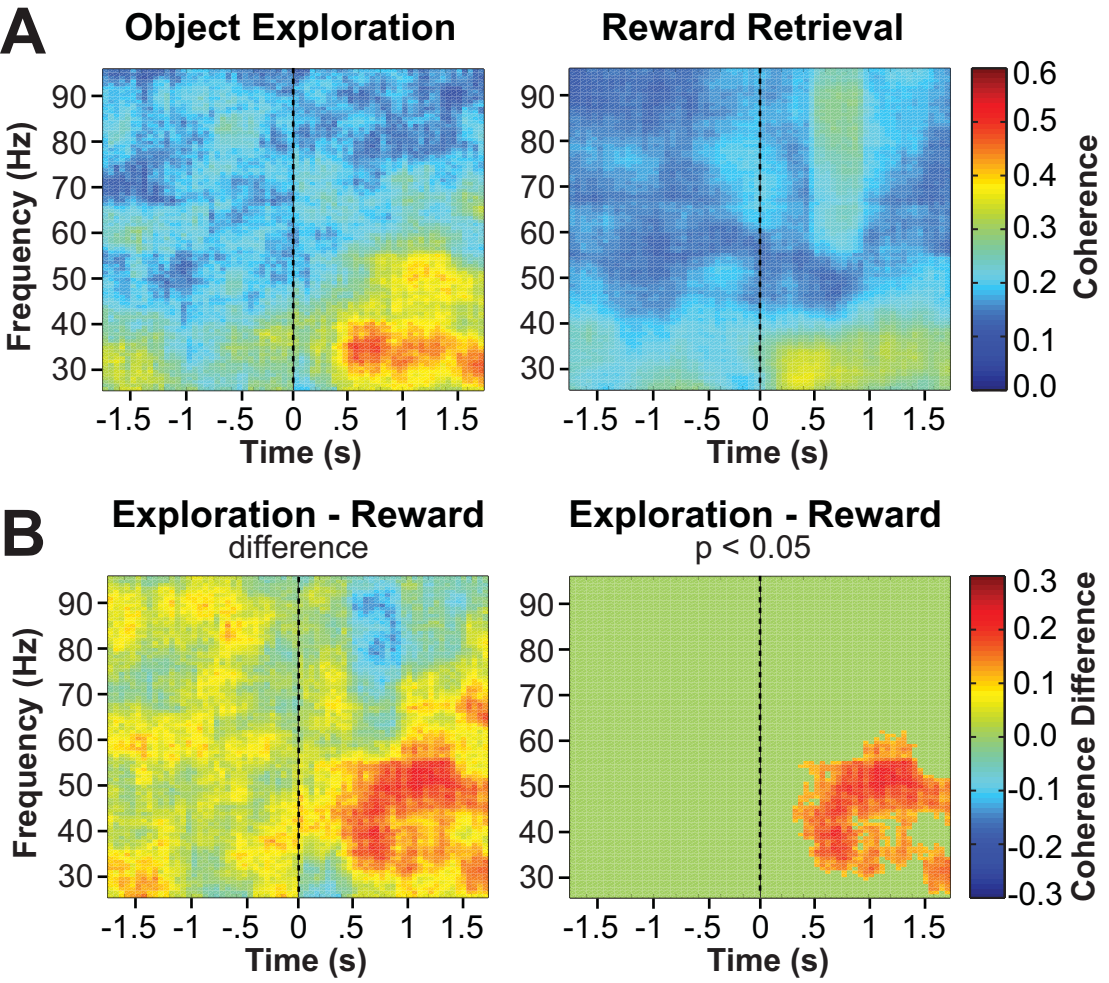
A
Object Exploration
Reward Retrieval
Frequency (Hz)
90
80
70
60
50
40
30
-1.5 -1 -.5 0 .5 1 1.5
Time (s)
0.6
0.5
0.4
0.3
0.2
0.1
0.0
Coherence
B
Exploration - Reward
difference
Exploration - Reward
p < 0.05
0.3
0.2
0.1
0.0
-0.1
-0.2
-0.3
Coherence Difference

Figure S3

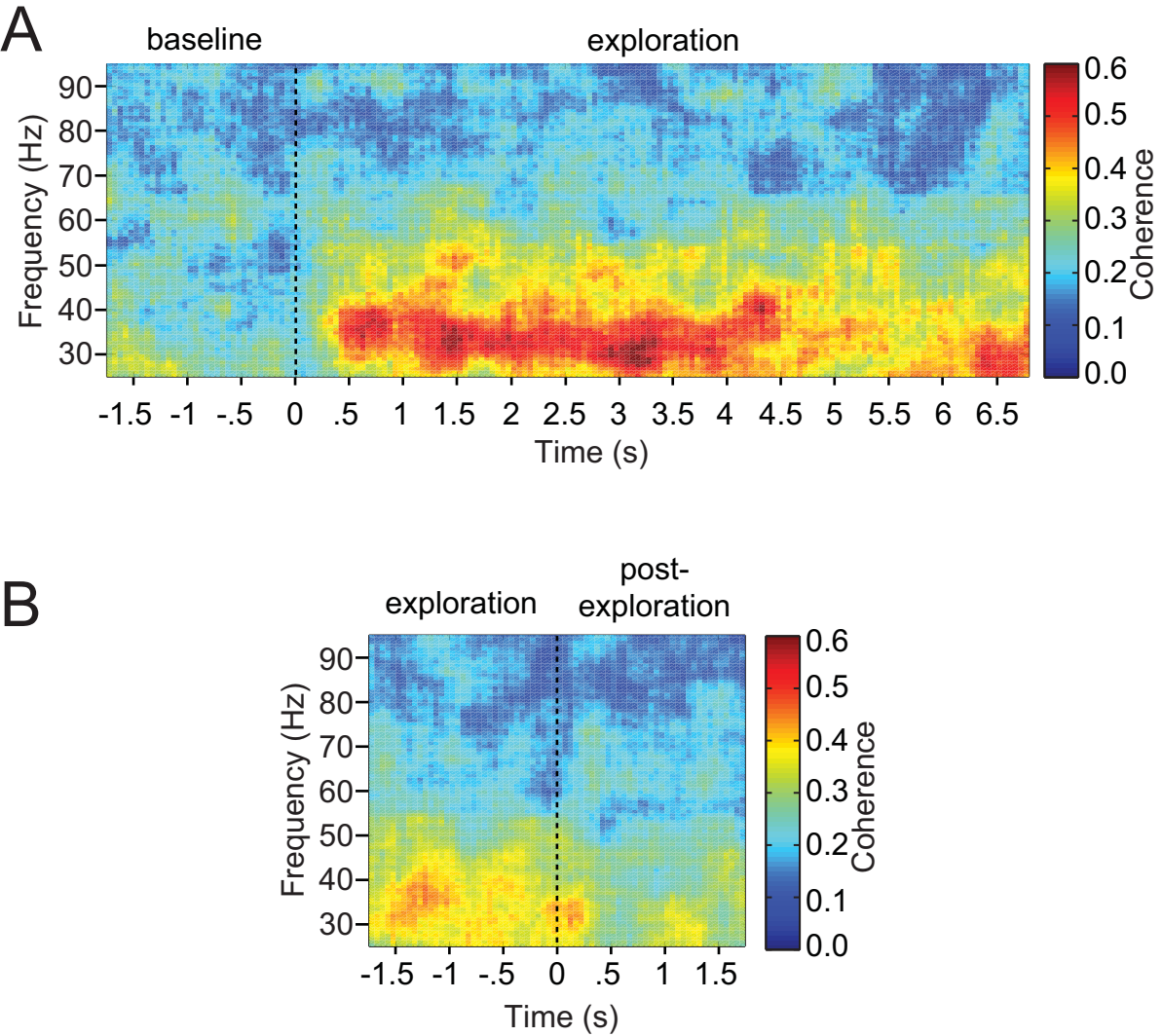
A
baseline
exploration
Frequency (Hz)
90
80
70
60
50
40
30
-1.5 -1 -.5 0 .5 1 1.5 2 2.5 3 3.5 4 4.5 5 5.5 6 6.5
Time (s)
0.6
0.5
0.4
0.3
0.2
0.1
0.0
Coherence
B
exploration
post-
exploration
Frequency (Hz)
90
80
70
60
50
40
30
-1.5 -1 -.5 0 .5 1 1.5
Time (s)
0.6
0.5
0.4
0.3
0.2
0.1
0.0
Coherence

Figure S4

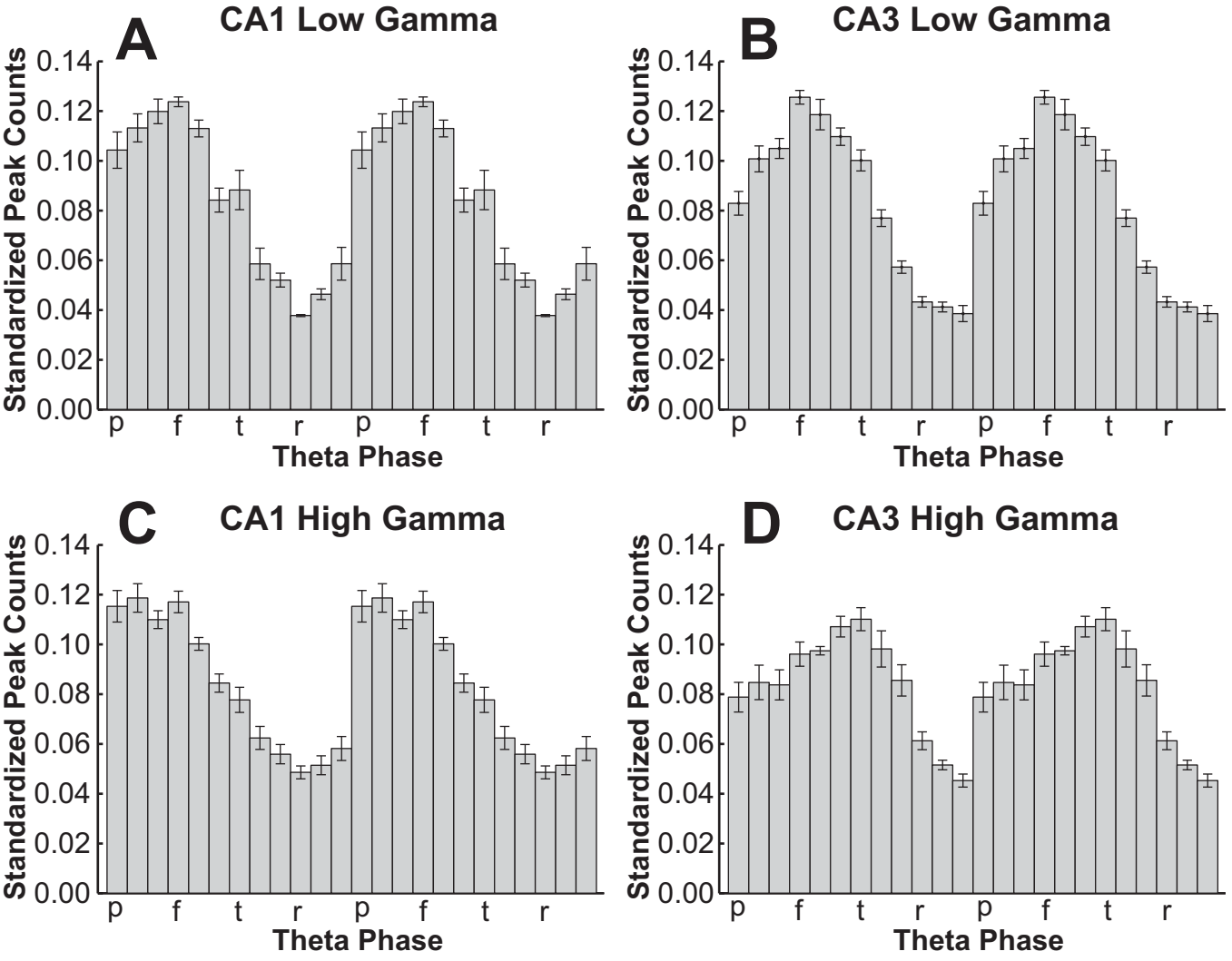
A
CA1 Low Gamma
B
CA3 Low Gamma
C
CA1 High Gamma
D
CA3 High Gamma
Standardized Peak Counts
0.00
0.02
0.04
0.06
0.08
0.10
0.12
0.14
p f t r p f t r
Theta Phase

Figure S5

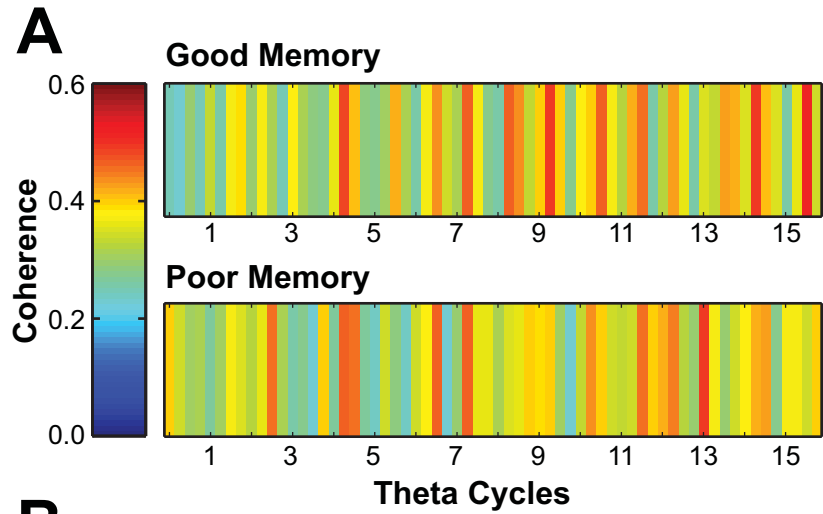
A
Good Memory
Poor Memory
Coherence
0.6
0.4
0.2
0.0
1
3
5
7
9
11
13
15
Theta Cycles

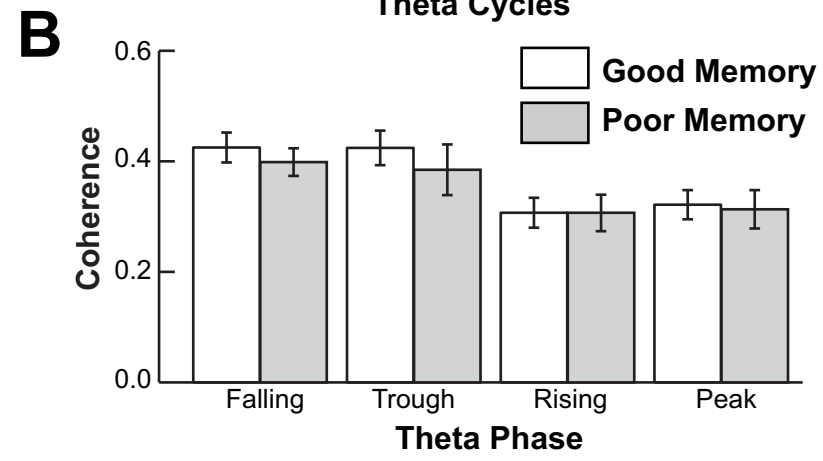
B
Good Memory
Poor Memory
Coherence
0.6
0.4
0.2
0.0
Falling
Trough
Rising
Peak
Theta Phase

Figure S6

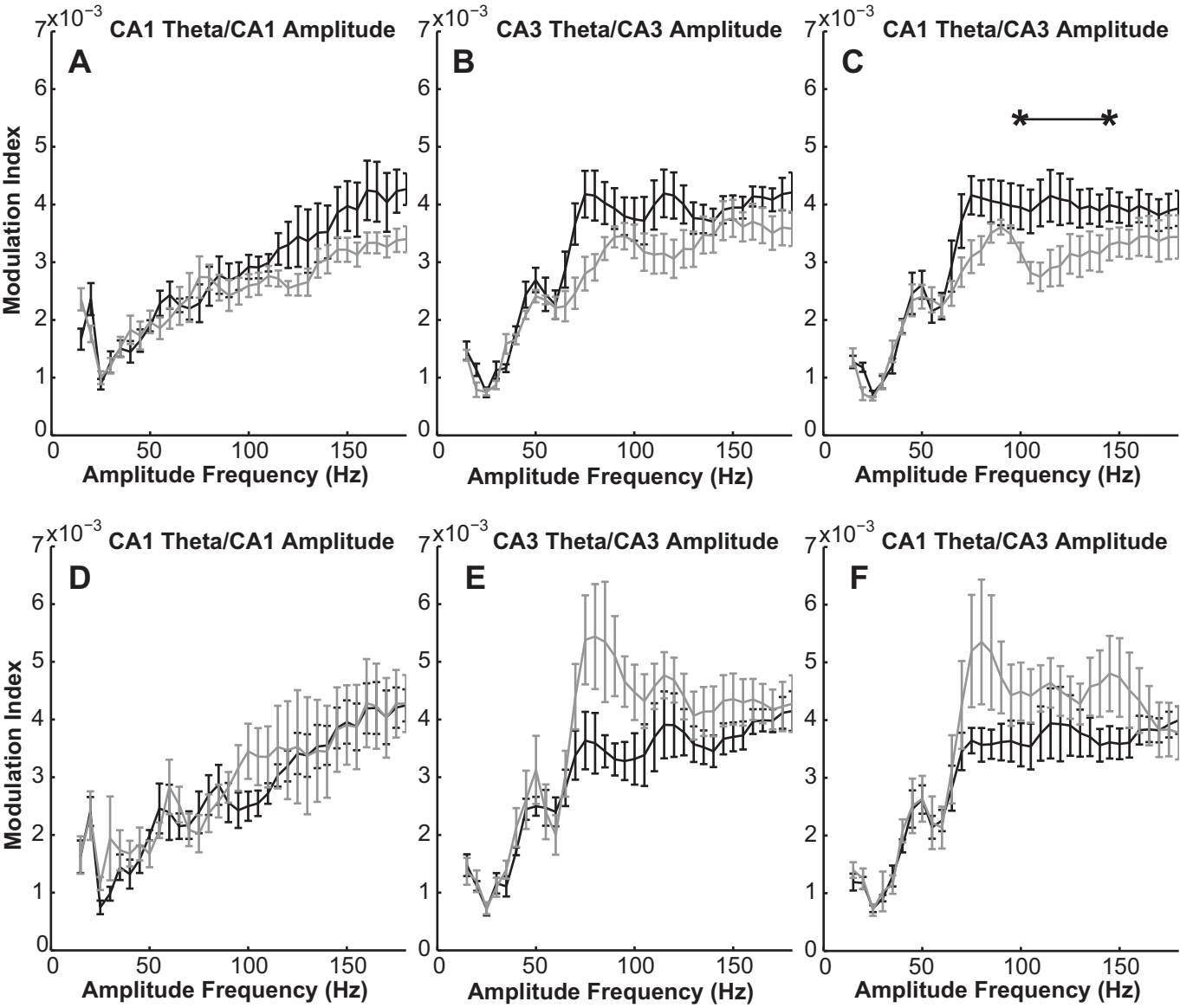
A
CA1 Theta/CA1 Amplitude
B
CA3 Theta/CA3 Amplitude
C
CA1 Theta/CA3 Amplitude
D
CA1 Theta/CA1 Amplitude
E
CA3 Theta/CA3 Amplitude
F
CA1 Theta/CA3 Amplitude
x10^-3
Modulation Index
Amplitude Frequency (Hz)
0
50
100
150
1
2
3
4
5
6
7
*
*

Supplemental Figure Legends

Figure S1. Coherence and phase coherence resulting from CA1 and CA3 field potential data randomly shuffled between novel object encounters. (**A**) The plots show mean coherence and phase coherence for exploration (black lines) and pre-exploration baseline (grey lines) periods. The levels of coherence and phase coherence for the randomly shuffled data are low for both exploration and baseline periods and no significant differences exist between conditions. (**B**) The plots show mean coherence and phase coherence for good memory (black lines) and poor memory (grey lines) conditions. The levels of coherence and phase coherence are low for both good memory and poor memory conditions and no significant differences exist between conditions. A small amount of theta coherence is visible in all of the plots, reflecting the contribution of (nonsynchronous) theta power in the cross spectrum to the coherence measurement and reflecting the chance level of within-event alignment of theta oscillations in the phase coherence measurement. Error bars show SEM.

Figure S2. Gamma coherence during novel object encounters and reward retrieval events. (**A**) A sliding window coherogram shows mean CA3-CA1 gamma coherence across rats during encounters with novel objects (onset = time 0) in which rats explored the objects for at least 2 s and during moments at the end of each lap when the rats retrieved a chocolate reward placed on the floor of the end of the central runway on the circle track (onset = time 0). The data for object exploration events are replotted from Figure 2A. The data for reward retrieval events show a small increase in low gamma coherence and perhaps a transient increase in coherence at higher frequencies. (**B**) The left panel shows the mean difference in CA3-CA1 coherence

between encounters with novel objects and reward retrieval events. The right panel shows clusters of data that exceeded statistical significance ($p < 0.05$) when evaluated using a permutation-approach that accounted for multiple comparisons (see Materials and Methods). A cluster in the low gamma range during exploration was the only data to reach statistical significance, indicating that the increase in gamma coherence during object exploration was greater than the increase in gamma coherence during reward retrieval events.

Figure S3. Gamma coherence during extended novel object encounters. (**A**) A sliding window coherogram shows mean CA3-CA1 gamma coherence across rats during encounters with novel objects (onset = time 0) in which rats explored the objects for at least 7.09 s (the mean object exploration time across rats). (**B**) A sliding window coherogram shows mean CA3-CA1 gamma coherence across rats during all encounters with novel objects (offset = time 0) in which rats explored the objects for at least 2 s. Coherence in the low gamma range remains elevated above baseline throughout exploration, although it may decrease to some extent towards the end of exploration.

Figure S4. Overall gamma amplitude by theta phase. Local field potentials across the entire recording session for both CA1 and CA3 were filtered for low and high gamma ranges, and for each range, counts of gamma peaks greater than 2 standard deviations above the mean were binned by waveform-based theta phase as recorded in CA1. Standardized peak counts (proportion of total peaks) were then averaged across rats for each bin. Data are plotted for two cycles of theta for improved visualization of the periodicity. The peak, falling, trough, and rising portions of the CA1 theta cycle are denoted as p, f, t, and r, respectively. Error bars show SEM.

Figure S5. CA3-CA1 low gamma coherence plotted by quartiles of theta phase and by memory performance. (**A**) Mean CA3-CA1 low (30-55 Hz) gamma coherence plotted for the first 16 CA1 theta cycles (lasting approximately 2 s) of novel object exploration. Each vertical stripe represents a quartile of the theta phase, and tick marks on the horizontal axes indicate the quartile centered on the peak of the theta wave. The appearance of banding for both good memory and poor memory conditions reflects the modulation of low gamma coherence by theta phase. (**B**) Mean CA3-CA1 low (30-55 Hz) gamma coherence during novel object exploration by theta quartiles. The level of coherence across quartiles of theta phase was similar between memory conditions. Error bars show SEM.

Figure S6. Phase-amplitude cross frequency interactions between the phase of theta oscillations (6-10 Hz) and amplitudes of higher frequencies (20 to 180 Hz). The data are plotted as a modulation index (Tort et al., 2010) that estimates the magnitude by which the phase of theta oscillations modulates the amplitude of higher frequencies. The top row (**A-C**) shows mean results for object exploration (black lines) and pre-exploration baseline (grey lines) periods. The bottom row (**D-F**) shows mean results for good (black) versus poor (grey) memory conditions. The left column (**A & D**), middle column (**B & E**), and right column (**C & F**) show CA1 theta phase-CA1 amplitude, CA3 theta phase-CA3 amplitude, and CA1 theta phase-CA3 amplitude cross-frequency relationships, respectively. The asterisks in (**C**) indicate a very high frequency range showing a statistically significant difference between exploration and baseline periods when evaluated using a permutation approach that accounted for multiple comparisons across

frequencies. No differences were observed in any comparison in the low gamma range. Error bars show SEM.